Experimental and Theoretical Electron Momentum Spectroscopic Study of the Valence Electronic Structure of Tetrahydrofuran under Pseudorotation

C. G. Ning,*,† Y. R. Huang,† S. F. Zhang,† J. K. Deng,*,† K. Liu,† Z. H. Luo,† and F. Wang*,‡

Department of Physics and Key Laboratory of Atomic and Molecular NanoSciences of MOE, Tsinghua University, Beijing 100084, People's Republic of China, and Centre for Molecular Simulation, Swinburne University of Technology, P.O. Box 218, Hawthorn, Melbourne, Victoria 3122, Australia

Received: May 02, 2008; Revised Manuscript Received: July 29, 2008

The most populated structure of tetrahydrofuran (THF) has been investigated in our previous study[17] using electron momentum spectroscopy (EMS). Because of the relatively low impact energy (600 eV) and low energy resolution ($\Delta E = 1.20$ eV) in the previous experiment, only the highest occupied molecular orbital (HOMO) of THF was investigated. The present study reports the most recent high-resolution EMS of THF in the valence space for the first time. The binding energy spectra of THF are measured at 1200 and 2400 eV plus the binding energies, respectively, for a series of azimuthal angles. The experimentally obtained binding energy spectra and orbital momentum distributions (MDs) are employed to study the orbital responses of the pseudorotation motion of THF. The outer valence Greens function (OVGF), the OVGF/6−311++G** model, and density function theory (DFT)-based SAOP/et-pVQZ model are employed to simulate the binding energy spectra. The orbital momentum distributions (MDs) are produced using the DFT-based B3LYP/aug-cc-pVTZ model, incorporating thermodynamic population analysis. Good agreement between theory and experiment is achieved. Orbital MDs of valence orbitals exhibit only slight differences with respect to the impact energies at 1200 and 2400 eV, indicating validation of the plane wave impulse approximation (PWIA). The present study has further discovered that the orbital MDs of the HOMO in the low-momentum region ($p < 0.70$ a.u) change significantly with the pseudorotation angle, ϕ, giving a v-shaped cross section, whereas the innermost valence orbital of THF does not vary with pseudorotation, revealing a very different bonding mechanism from the HOMO. The present study explores an innovative approach to study pseudorotation of sugar puckering, which sheds a light to study other biological systems with low energy barriers among ring-puckering conformations.

I. Introduction

The determination of electronic structures of isolated fragments of DNA is an important step toward the understanding of mechanisms for secondary structures of DNA and its damage.[1] Tetrahydrofuran (THF, C_4H_8O) has an aromatic heterocyclic and saturated five-member ring, which can be regarded as a prototypical structural unit[2] of the sugar moiety in the sugar−phosphate backbone of DNA and RNA.[3] When the sugar moiety connects through the glycosyl N−C bond with a nucleic acid base (NAB), it forms nucleosides, an important class of anti-HIV and anti-AIDS drugs. For example, a derivative of THF, azidothymine, is commonly recognized as the first anti-AIDS drug used in antiviral chemotherapy and prophylaxis in the United States.[4] (Revised: July 29, 2008).

Like other molecules with a five-member ring, THF is not planar but puckered. It displays an internal motion known as pseudorotation,[5] which was originally postulated for cyclopentane.[6] Conformations of THF are flexible along the pseudorotation path[7,8] as a function of the pseudorotation angle ϕ. The nearly free pseudorotation and several minima, which are separated by very low energy barriers, appear in a 2π range of the potential energy surface. For example, the THF conformers at $\phi = 0°$ and 180° possess a C_s symmetry (E, envelope), global minima, whereas conformers at $\phi = \pm 90°$ exhibit a C_2 symmetry (T, twisted), local minima.[9]

A number of theoretical and experimental studies[1,7−18] have tackled THF. However, the findings largely depend on the models used (theory) and methods of experimental data analysis. This is due to the small and subtle energy differences among the conformations produced by pseudorotation of tetrahydrofuran, which are within the error bars of many quantum mechanical models. In addition, the size of the THF molecule prohibits higher-level quantum mechanical models with appropriate basis sets. In our previous work, the most populated conformer of THF was recognized as the C_s conformer, on the basis of the orbital MDs of the HOMO observed using electron momentum spectroscopy (EMS),[17] in agreement with recent results of Rayon and Sordo using high-level ab initio models.[9]

EMS features in the binding energy spectra as well as the ability of orbital images. When combined with quantum mechanics, EMS provides *additional* information of orbital-based valence electronic structures to the majority of energy focused approaches.[19−27] Previous studies have established that EMS is an attractive technique to investigate conformations of organic molecules and small biomolecules.[17−21,28−33] It has been demonstrated that the symmetries of the HOMOs with respect to the minimal structures of C_s and C_2 on the potential-energy surface (PES) produced by pseudorotation differentiate the conformers of THF.[17] This finding is further supported by a

* To whom correspondence should be addressed. E-mail: ningcg@tsinghua.edu.cn (C.G.N.), djk-dmp@tsinghua.edu.cn (J.K.D.), fwang@swin.edu.au (F.W.).
† Tsinghua University.
‡ Swinburne University of Technology.

10.1021/jp8038658 CCC: $40.75
Published on Web 10/09/2008

detailed theoretical analysis of the individual valence orbitals of the three important structures, C_s, C_2, and C_1 produced by pseudorotation of THF.[18] However, an orbital-based study of valence electronic structure of THF as a function of pseudorotation, which will contribute significantly to our understanding of this difficult issue of sugar puckering in biochemistry, does not exist.

In the development of EMS technique,[34,35] it has focused on the study of valence electronic structures of molecules with a clearly defined minimum structure.[36] The technique has been recently applied to study conformations of organic and biomolecules,[31] which are characteristic configurations on the potential energy surfaces.[17−20,33] It is possible in reality that all configurations, including the energy local minimum states and transition states on the PES, contribute to the electron density distributions according to the Boltzmann distribution under the experimental conditions. The previous EMS studies of THF[17,18] concentrated on the isolated characteristic configurations on the PES. However, because of the low-energy barriers, the transition states produced by pseudorotation, such as the C_1 conformation of THF could be also populated at room temperature. As a result, the experimental results may be more appropriately simulated if the Boltzmann distribution of the structures of THF is also considered.

Our previous EMS experiment[17] was unable to resolve the outer valence electronic structure of THF due to the low impact energy of 600 eV (plus binding energy), which is associated with a low-energy resolution of $\Delta E = 1.2$ eV. In the present work, a high-resolution EMS experiment of THF in valence space is achieved using a significantly improved experiment energy resolution of $\Delta E = 0.68$ eV, with impact energies of 1200 and 2400 eV, plus binding energies. The latter energies are sufficiently high to obtain converged momentum information.[37−41] The present study is, therefore, able to provide more detailed information for the valence electronic structures in the study of THF pseudorotation to support our theoretical analysis.

II. Theory and Experimental Details

Electron momentum spectroscopy (EMS) is a binary (e, 2e) experiment in which an incident electron with high enough energy E_0 induces ionization of a molecular target.[34−36,42] The scattered and ionized electrons are subsequently detected in coincidence at equal kinetic energies and equal polar angles, that is, $E_1 \approx E_2$, and $\theta_1 = \theta_2 = 45°$, and therefore equal momentum $p_1 \approx p_2$. The initial momentum p of the knocked-out electron obeys, therefore, a simple conservation rule,

$$p = \{(2p_1 \cos\theta_1 - p_0)^2 + [2p_1 \sin\theta_1 \sin(\varphi/2)]^2\}^{1/2}, \quad (1)$$

where p_0 is the momentum of the incident electron, and φ is the azimuthal angle between the two outgoing electrons. Note that the azimuthal angle, φ, and the pseudorotation angle, ϕ, are completely different quantities.

Under the assumptions of the Born (sudden or vertical), binary encounter, and plane wave impulse approximations (PWIA), the triple differential EMS cross-section for randomly oriented molecules is then given by

$$\sigma_{\mathrm{EMS}} \propto \int \mathrm{d}\Omega |\langle \nu_{\vec{p}} \Psi_f^{N-1} | \Psi_i^N \rangle|^2, \quad (2)$$

where $\nu_{\{\vec{p}\}}$ represents a plane wave function $e^{i\vec{p}\cdot\vec{r}}$. The overlap of the ion and neutral wave functions in eq 2 is referred to as a Dyson orbital.[43−45]

Dyson orbitals are solutions of the Dyson equation, which can be approximated by solutions from configuration interaction (CI)[46] or Green's function (GF) calculations.[45] Assuming a depiction of ionization events at the level of Koopmans' theorem, Dyson orbitals most naturally reduce to Hartree−Fock (HF) orbitals (target HF approximation, THFA) with a spectroscopic strength of 1. Dyson orbitals can also be approximated using the target Kohn−Sham approximation (TKSA) from relevant Kohn−Sham orbitals.[47] With the THFA or TKSA, and upon accounting for the dispersion of the ionization intensity over shakeup and shake-off satellites, eq 2 then simply becomes,[47,48]

$$\sigma_{\mathrm{EMS}} \propto S_i^f \int \mathrm{d}\Omega |\psi_i(p)|^2, \quad (3)$$

where $\psi_i(p)$ represents orbital i in the momentum space, that is, the Fourier transform of a canonical HF or KS orbital, and S_i^fdenotes the associated pole strength. The electron correlation of the ground electronic state for a molecule with a closed shell is included in the Kohn−Sham orbital through the exchange-correlation potential.[47]

The theoretical simulations of the orbital MDs are convolved the experimental resolution at $E_0 = 1200$ eV using a Monte Carlo method.[49] It should be noted that the momentum resolution depends on the impact energy E_0. The momentum resolution of $E_0 = 1200$ eV is $\Delta p \sim 0.16$ au(fwhm), and $\Delta p \sim 0.23$ au(fwhm) at 2400 eV. As the intensities of the experimental orbital MDs are obtained in a relative scale, a proper normalization process must be employed. The present study uses one of the common normalization processes in the area of EMS. That is, a normalization constant was determined by the best fit between the experimental summation of the outer valence orbital MDs, that is, peaks 1−4 in the binding energy spectrum (the bottom panel of Figure) and the corresponding summation of the simulated MDs of orbital 20−11 in the outer valence space of THF. Then, this constant was used to normalize the experimental distributions for each peak.

The theory of electron momentum spectroscopy (EMS) assumes that the collision operator depends only on electronic degree of freedom,[36] with an averaged rotational state and a ground-state vibrational average at the equilibrium of the nuclear positions. A vibrationally resolved method such as the EMS analysis of ethylene by Brion and Davidson et al.[50] is not applicable to larger molecules like THF. In addition, it has been demonstrated[50] that vibrational effects are very small and do not significantly change the orbital MDs of a rigid molecule. In the present study, we estimate the effects on orbital MDs with respect to pseudorotation of THF using a simple model. The population distribution $f(\phi)$ of a state at a temperature T and energy $V(\phi)$, is given by the Boltzmann distribution as

$$f(\varphi) = g(\varphi) e^{-\frac{V(\varphi)}{kT}}, \quad (4)$$

where k is the Boltzmann constant, ϕ is the pseudorotation angle, and $g(\phi)$ is a weight function. This equation holds valid when the vibrational energy gap $\hbar\omega \ll kT$. The momentum distribution, $\rho_i(p)$, for the ith ionized state is given by

$$\rho_i(p) = \int_0^{2\pi} f(\varphi) \rho_i(p, \varphi) \mathrm{d}\varphi, \quad (5)$$

where $\rho_i(p, \phi)$ is the momentum distribution of the ith ionized state of the THF conformation with a pseudorotational angle ϕ.

To explore the pseudorotation angle ϕ dependency on the orbital MDs of specific valence orbitals, a flexible model suggested by Meyer et al.[8] is, therefore, employed to generate a series of conformations without further optimization. The

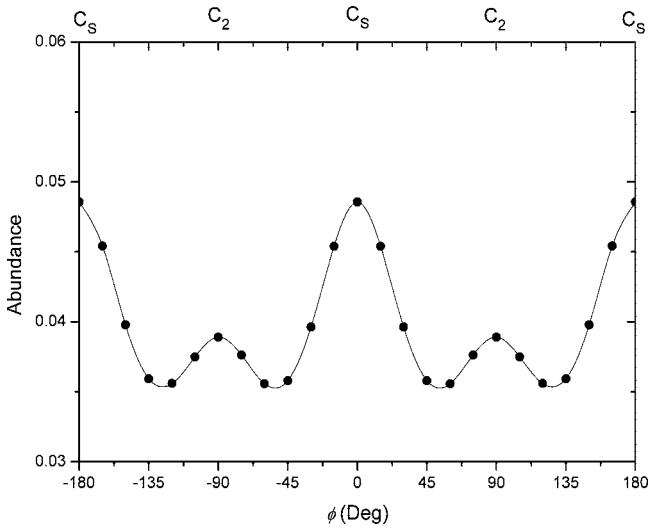

Figure 1. Population distributions of THF at the room temperature of $T = 298$ K.

variables are determined using the high level calculated data of C_2 and C_s given by ref 9. The single-point electronic calculations are performed with a step of $\Delta\phi = 15°$ using the hybrid DFT-based B3LYP/aug-cc-pVTZ model,[51] which is incorporated in the *Gassian03* computational chemistry package.[52] A program named ***NEMS***[53] was recently developed in Tsinghua University and was employed to generate the theoretical momentum distributions. The ***NEMS*** program uses a general analytical formula to handle basis functions, regardless angular momentum quantum numbers.[53]

The EMS spectrometer constructed in the laboratory of Tsinghua University takes symmetric noncoplanar geometry. It uses a double toroidal energy analyzer and position sensitive detectors to achieve the energy and angle multichannel detections.[54,55] Recently, significant modifications have been implemented on the spectrometer to achieve higher resolution.[56] Briefly, an electron gun equipped with the oxide cathode, which worked at a much lower temperature than the generic filament cathodes, is used to generate the electron beam with low energy spread and low divergence angle. The electron beam size is constrained to 0.3 mm in diameter by a molybdenum aperture. The passing energy is set to 50 eV for improving the momentum resolution and energy resolution. With these measures and optimization of electron optics using the Monte Carlo simulation, the angle resolutions, $\Delta\varphi = \pm 0.84°$ and $\Delta\theta = \pm 0.53°$, are obtained by standard calibration run for argon. The energy resolution highly depends on the emitting current of the cathode due to the space charge effects. In the present work, an energy resolution of $\Delta E = 0.68$ eV (fwhm) is obtained.[53,56]

The THF sample is a commercially available product with a claimed purity of 99.9%. The measurement, therefore, proceeded without further purification. No impurity of the sample is evident in the binding-energy spectra.

IV. Results and Discussion

IV.1. Pseudorotation Angle ϕ-Dependent Conformation Population. Population of the THF conformations produced by pseudorotation reveals their energy dependence at a given temperature. Estimated abundance distributions according to the pseudorotation angle ϕ at the temperature of $T = 298$ K is given in Figure 1, where the pseudorotation potential $V(\phi)$ is based on the work of Rayon and Sordo,[9] and the weight function $g(\phi)$ is approximated as a constant, independent of ϕ in the present work. Figure 1 indicates that all conformations including the minimum energy states and transition states are populated under the given conditions. As a result, all conformations under the experimental conditions may contribute to the observed results with a dominance of the local minimum energy structures.

In the valence space, THF possesses 30 valence electrons, which doubly occupy 15 orbitals in the electronic ground state. Because of the associated changes in point-group symmetries of the conformations when the pseudorotation angle ϕ varies, these valence orbitals are labeled according to the orbital energy ordering (Table 1) rather than the symmetry-based labels in the following discussion. For example, HOMO is orbital 20. The valence orbitals of THF are further divided into outer valence orbitals (orbital ionization potential (IP) < 18 eV, i.e., orbitals 20−11) and inner valence orbitals (orbital IP > 18 eV, i.e., orbitals 10−6), which are approximately determined by break of the OVGF picture.

IV.2. Density Map and Binding Energy Spectra of THF. The observed EMS momentum−energy (M-E) density map of THF at the electron impact energy of 1200 eV plus binding energy is given in Figure 2. Electron binding energy spectra can be inferred from this density map for each azimuthal angle, which defines the momentum of the electron prior to ionization. Inversely, the angular dependence of ionization intensities can

TABLE 1: Ionization Potentials of the Valence Orbitals for THF (in eV)

orbital no.	OVGF/6−311++G**[a]	$\Delta E_{max-min}$	SAOP/et-pVQZ[b] C_s, C_2	PES[c]	EMS[d]
20	9.89, 10.16	0.27	10.61, 10.30	9.74	9.7 (1.00)
19	11.38, 11.89	0.51	12.21, 11.96	11.52	12.1 (1.00)
18	11.76, 12.23	0.47	12.21, 12.36		
17	11.70, 12.29	0.59	12.63, 12.77	12.52	
16	12.60, 13.18	0.58	12.96, 13.00		
15	14.07, 14.15	0.08	14.10, 14.25	14.1	14.5 (1.00)
14	14.53, 15.01	0.48	14.49, 14.74	14.5	
13	15.05, 15.64	0.59	15.39, 15.04	15.4	
12	16.71, 16.87	0.16	16.25, 16.49	16.8	16.7 (1.00)
11	17.07, 17.25	0.18	16.57, 16.78		
10			18.91, 18.90	19.5	19.7 (0.75)
9			19.16, 19.14		
8			22.49, 22.72		23.4 (0.45)
7			23.71, 23.87		24.6 (0.56)
6			30.31, 30.60		31.8 (0.40)

[a] The variation ranges of ionization energies calculated at a series of pseudorotation angles ϕ using the OVGF/6−311++G** model, and the maximum differences among the ionization energies are listed in column $\Delta E_{max-min}$. See text for details. [b] See ref 18. [c] See ref 58. [d] The values in parentheses are the pole strength. The normalization procedure takes the pole strength of the outer valence orbitals as one.

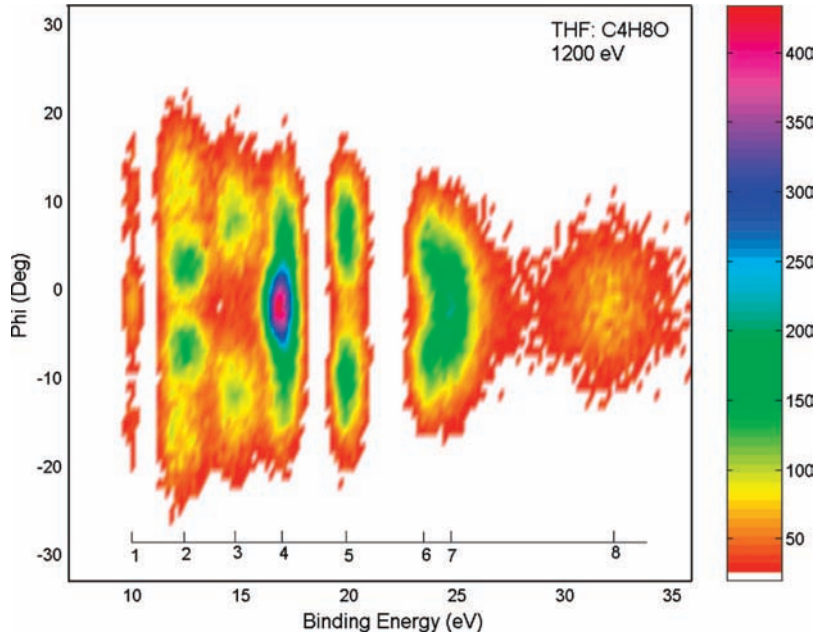

Figure 2. (Color online) Valence momentum−energy density map of tetrahydrofuran measured at the impact energy of 1200 eV plus binding energy.

be used to reconstruct the experimental electron momentum distributions associated to specific ionization channels.[57] The overall characters, of the M-E density map, although qualitative, provide useful information for the later orbital assignment of the binding energy spectra.

Individual or group of ionization states can be observed qualitatively in the density map. For example, the M-E density distributions shown in Figure 2, which are associated with ionization states in the binding energy region of approximately 10−25 eV, labeled as 1−7 respectively, are resolved. The ionized states, which show a maximum at the momentum origin (or zero azimuthal angle, φ), are likely s-electron dominant states, such as the state labeled 4. In contrast, the p-electron dominant states usually exhibit a bell-shaped cross section. That is, the density starts at a minimum at the momentum origin, increases as momentum (azimuthal angle) increases in value $|\varphi|$, until it reaches a maximum at a nonzero momentum value, such as the state labeled 2. Two different types of orbitals could be related to the states located at ∼25 eV, which are labeled 6 and 7. No clear boundary exists between the states at this energy location, but the states can be differentiated from their individual symmetries if they are different. Resolution of the spectrometer is indicated by the separations of the density peaks in this M-E density map.

On the basis of the information provided by the M-E density map at various azimuthal angles, the measured (e, 2e) binding energy (ionization) spectrum of THF is given in Figure 3 (bottom panel), together with the simulated spectra using the OVGF method and the DFT-based SAOP/et-pVQZ model.[18] The experimental binding-energy spectrum is recorded in a range of 7−37 eV at the impact energy of 1200 eV plus binding energies, which are obtained through the integration of the electron density map in Figure 2 over all azimuthal angles.

The orbital based discrete binding energies are then obtained by fitting the observed spectra in Figure 3 into Gaussian functions (the dashed lines in the bottom panel). The centers of the Gaussian peaks, which give the orbital ionization potentials (IPs), are estimated on the basis of a photoelectron spectroscopy (PES) measurement[58] with small adjustments to compensate

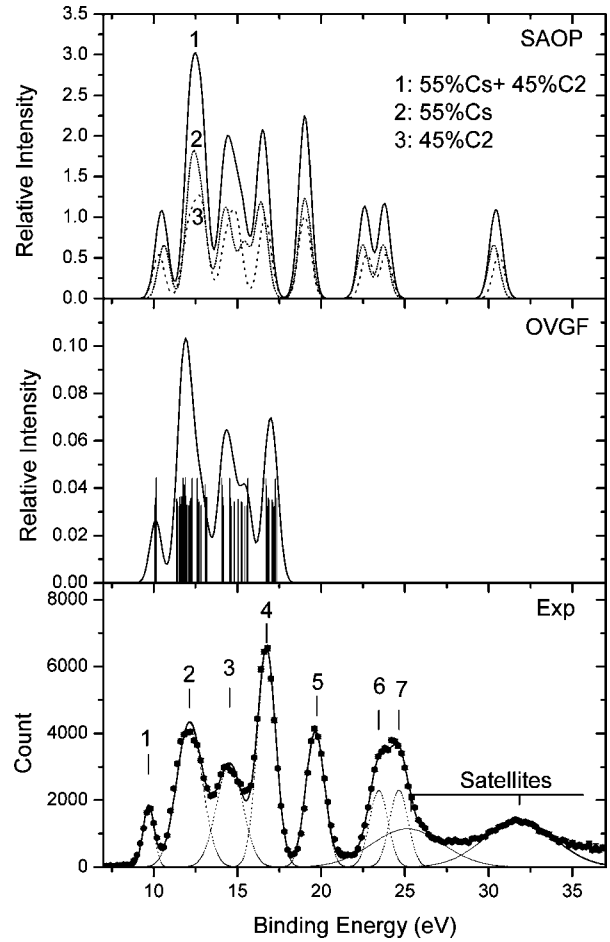

Figure 3. Binding energy spectra of THF. Experimental binding energy spectrum (bottom panel) is obtained by summing over all ϕ angles. The simulated spectra using the OVGF/6−311++G** (middle panel) and the DFT-SAOP/et-pVQZ model (top panel) are also given.

asymmetry in the shape of the Franck−Condon envelopes. The orbital IPs so obtained are listed in Table 1, taking into account of Franck−Condon widths (folded with the EMS instrument

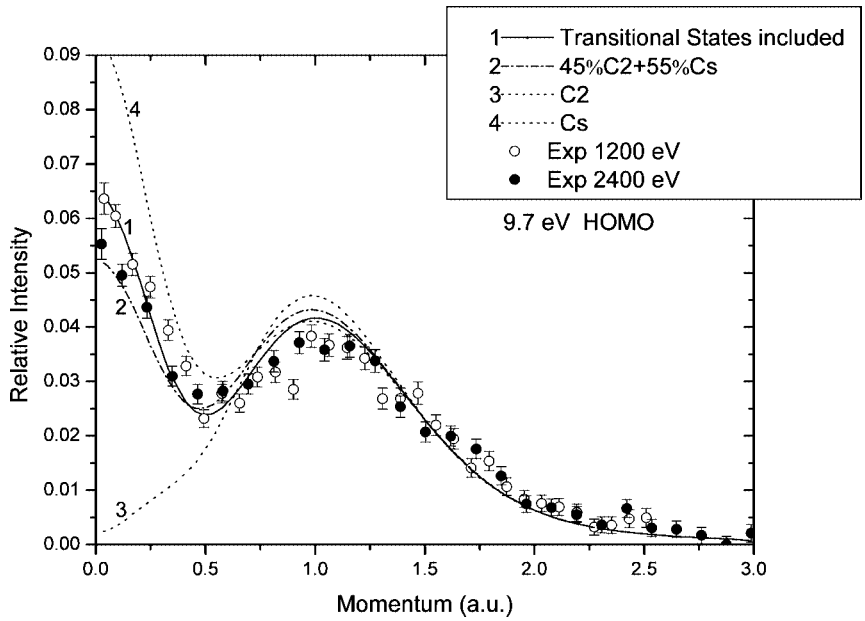

Figure 4. Convolved and spherically averaged momentum distributions of the HOMO orbital MDs of tetrahydrofuran at an impact energy of 1200 and 2400 eV plus binding energy.

energy resolution of 0.68 eV fwhm). The first peak centered at 9.7 eV is related to the HOMO of THF, which is clearly resolved from other valence states. The new EMS binding energy spectra of THF obtained in the present study provide solid information to support our earlier assignment that the small spike in the binding energy spectrum under an impact energy of 600 eV[17] is indeed the signature of the HOMO rather than background noise.

Figure 3 also reports two simulated binding energy spectra of THF. One is obtained using the OVGF/6−311++G** model (middle panel), the other is obtained using the DFT-SAOP/et-pVQZ model (top panel). The simulated spectra are obtained by convoluting the contributions from individual lines (given in Table 1) by a Gaussian shape function with an fwhm of 0.8 eV to best reproduce the experimental spectrum. The intensities (i.e., the heights of the spikes) in the OVGF spectrum are proportional to the computed pole strengths and the relative abundance given by eq 4, whereas the intensities in the DFT-SAOP/et-pVQZ calculations are synthesized using the 55% Cs (global minima) and 45% C2 (local minima) of THF. It is seen from Figure 3 that the simulated spectra of THF agree well in the outer valence space with the experimental binding energy spectrum in both peak positions and intensities. When the energy moves into the inner valence shell, for example, IP > 18 eV, the OVGF model is not so useful due to its limitations. However, the DFT-SAOP/et-pVQZ model[18] is able to reproduce reliable binding energies in the entire valence space for THF.

Table 1 reports the valence orbital ionization energies of THF observed in the EMS experiment, with comparisons to a previous PES experiment and quantum mechanically calculated IPs. The calculated IPs using the OVGF/6−311++G** model (IP < 18 eV) and the DFT-SAOP/et-pVQZ model (IP < 35 eV) are based on the geometries optimized at the MP2/aug-cc-pVTZ model.[9] In the OVGF/6−311++G** calculations, the present study calculates the IPs of THF at a series of pseudorotation angles ϕ, in the range of 0−180° at a step of 15°. Only the maximum and minimum of ionization energies for each orbital are listed in Table 1.

On the basis of the OVGF/6−311++G** calculations, the outer valence IPs of THF vary in a range of 0.2−0.6 eV due to the pseudorotation of THF, shown in Table 1. The orbital-based IP variations are significantly larger than the energy difference of 72 cm^{-1} (ca. 0.01 eV) between the conformers. The latter is predicted by the MP2/aug-cc-pVTZ calculations[9] with an extrapolation to the complete basis set (CBS) limit.[9] As a result, a realistic simulation of the experimental spectrum for THF needs to consider the ϕ dependence of the conformation contributions to the ionization binding energy spectrum.

IV.3. Pseudorotation Mechanism Revealed from the HOMO. The highest occupied molecular orbital (HOMO) of THF is remeasured in the present study with a clear energy resolution at higher impact energies of 1200 and 2400 eV, respectively, plus binding energies. The findings are demonstrated in Figure 4, together with the high-resolution experimental momentum distributions and the simulated using the method described in eq 5 under the room temperature of $T =$ 298 K (curve 1). A slightly different orbital MDs of the HOMO at 1200 and 2400 eV impact energies (plus binding energies) are observed in a very low momentum region of ca. $p < 0.25$ au, as seen in Figure 4. Such a difference in orbital MDs is dominated by the impact-energy-dependent momentum resolutions (e.g., $\Delta p \sim 0.16$ au (fwhm) at 1200 eV and $\Delta p \sim 0.23$ au (fwhm) at 2400 eV), rather than the distorted wave effects in this momentum region, which is supported by recent studies of oxygen[37] or ethylene molecules.[38] More importantly, Figure 4 clearly indicates significantly different symmetries of the HOMOs between the two competitive conformers of THF, C_s, and C_2, which supports our earlier conclusion that the C_s conformer of THF is the dominant one at the experimental conditions.[17]

As discussed earlier,[17,18] the HOMO of THF plays a particularly important role, which differentiates the conformers produced by the pseudorotation motion. The orbital MDs of the HOMOs of C_s and C_2 reveal the significant differences in their symmetry and, as a result, identify the dominant conformer for THF. The MDs of this orbital have been simulated as a function of the pseudorotation angle ϕ, which are given in part a of Figure 5. In this figure, the simulations are based on the experimental conditions in the region of [0°, 180°] with an interval of $\phi = 15°$. Note that the orbital MDs of the global

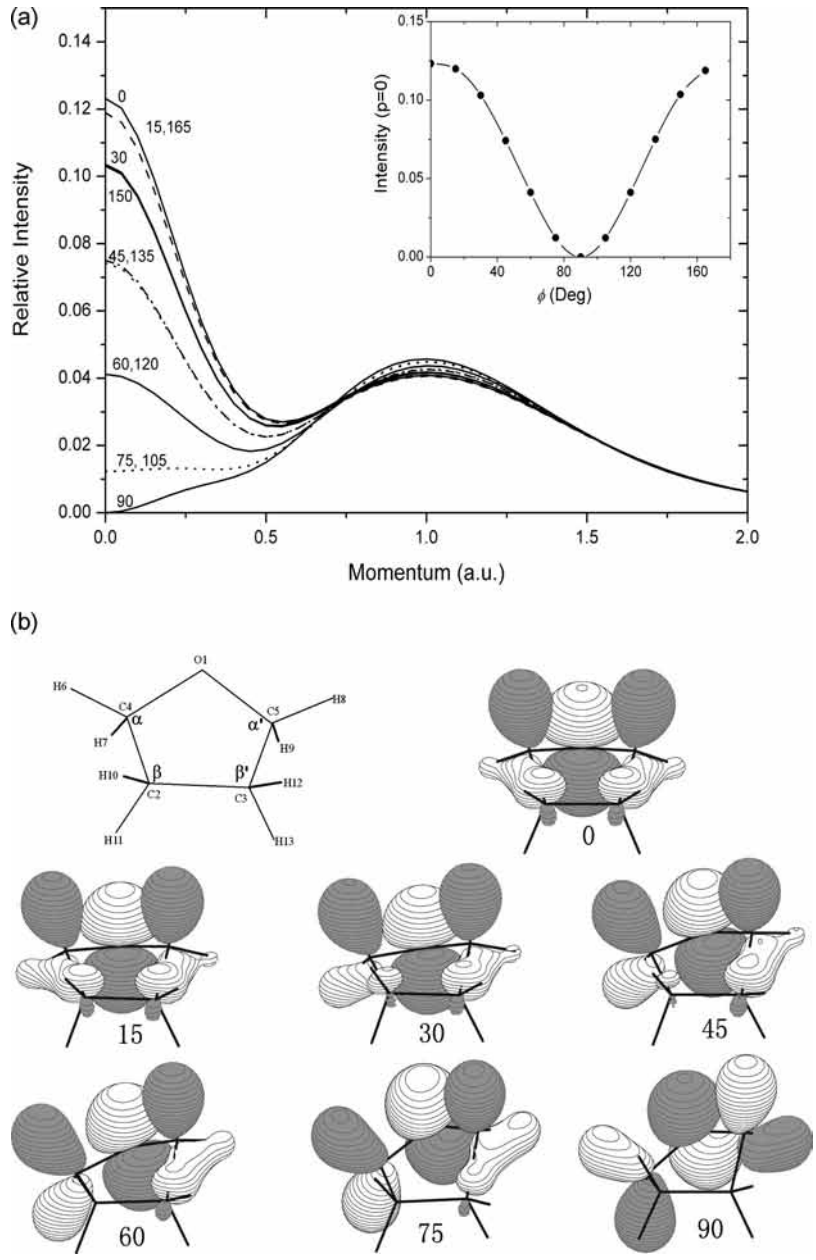

Figure 5. (a) Simulated MDs of the HOMO orbitals of tetrahydrofuran at various pseudorotation angles (ϕ). The intensity cross section at the momentum origin $p = 0$ versus the pseudorotation angle ϕ is given by the insert (b) The density distribution of HOMO of tetrahydrofuran at the pseudorotation angles of 0, 15, 30, 45, 60, 75, and 90°, using *Molden 4.3* by using density contour value (0.05).[60]

minimum structure of THF (C_s) corresponds to the curve (the solid line at the top) at $\phi = 0°$ in this figure, the local minimum structures C_2 are associated with the orbital MDs with respect to $\phi = \pm 90°$, whereas the transition states C_1 correspond to the MDs at $\phi = \pm 45°$ and $\phi = \pm 135°$, respectively.

In part (a) of Figure 5, the orbital MDs of the HOMOs reveal the orbital-based pseudorotation mechanism at the low momentum region of $p < 0.70$ au with a maximum difference at the momentum origin of $p = 0.0$ au. The orbital MDs of the HOMOs join at $\phi = 90°$ (C_2 symmetry conformer, a local minimum structure) from opposite directions when approaching $\phi = 90°$, giving a v-shaped cross section as indicated in the insert panel of part (a) of Figure 5. When $\phi < 90°$, orbital MDs of the HOMOs decrease as ϕ increases in the low momentum region, reach the bottom of the well at $\phi = 90°$, and then increase as ϕ increases in the region of $\phi > 90°$.

In the region of low momentum, p, the wave functions correspond to the long range, r, in position space. Part (a) of Figure 5 reveals that dominant orbital distortions in HOMO appear in the long-range region due to the pseudorotation. The v-shaped curve (the inset in part (a) of Figure 5) presents the cross sections of the maximum distortion of the HOMOs at the momentum origin, $I(\phi, p = 0)$, with respect to the pseudorotation angle, ϕ in the angular region of 0−180°. For example, the envelope like structures of $E_\alpha(C_1)$ and $E^{\alpha'}(C_1)$ at $\phi = 45$ and 135°, respectively, which locate on either sides of the MD minimum of $\phi = 90°$ ${}^{\beta}T_{\beta'}(C_2)$, are equivalent structures after spherical average. The inversion-produced structures, $E_\alpha(C_1) \rightarrow E^{\alpha'}(C_1)$, contain ϕ-dependent distortions in their orbital wave functions. As a result, the HOMO MDs reflect certain subtle differences in the pseudorotation of THF.

Knowing the subtle distortions in the orbital MDs of the HOMOs of THF in momentum space, the present study proceeds to correlate the HOMOs in a more familiar coordinate space, within the concept of dual space analysis (DSA).[18] Part (b) of Figure 5 gives the orbital electron density contours of the

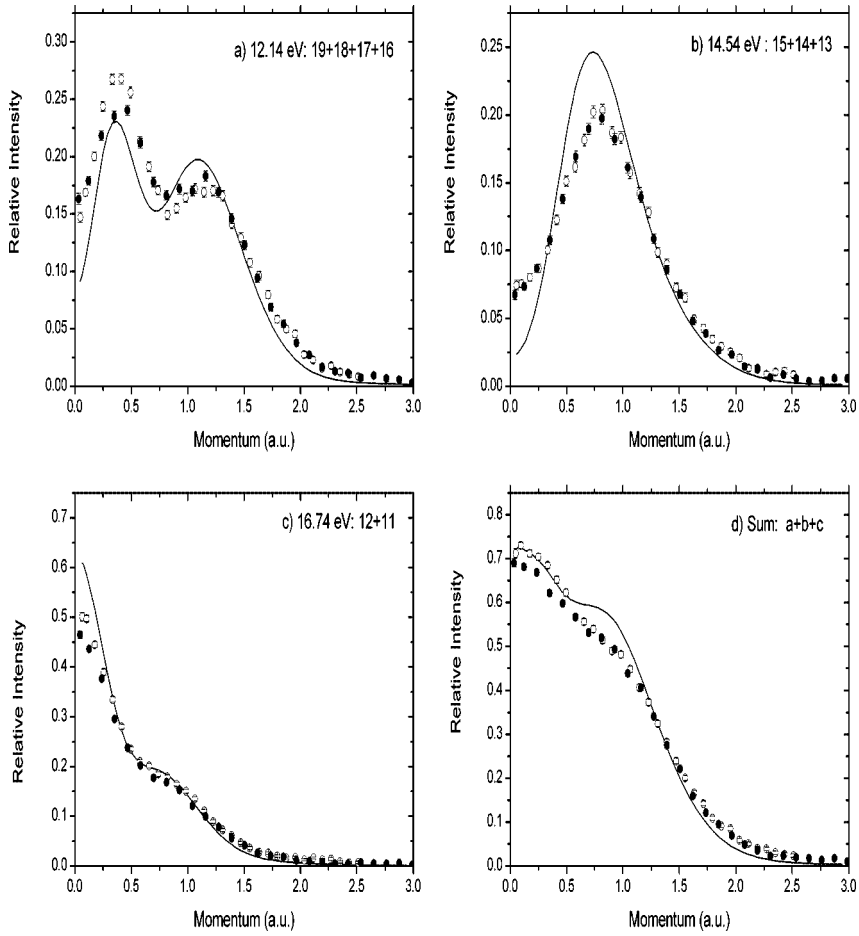

Figure 6. Comparison of the synthesized MDs of the outer valence orbitals of tetrahydrofuran (IP < 18 eV) with the observed spectra at an impact energies of 1200 eV (open circles) and 2400 eV (solid circles) plus binding energies, respectively.

HOMOs as a function of the pseudorotation angle ϕ at 0° (C_s), 15°, 30°, 45° (C_1), 60°, 75°, and 90° (C_2), which represent half of the angles in part (b) of Figure 5 due to the symmetry at $\phi = 90°$ (part (a) of Figure 5, insert). As indicated previously,[18] the HOMOs of THF at various ϕ angles are indeed dominated by O(2p) + H(1s) orbitals, resulting in an $s^x p^y$-hybridized orbital MDs in momentum space (part (b) of Figure 5 at 0°, i.e., the HOMO density distributions of the C_s conformer of THF). In fact, the HOMO of the C_s conformer is dominated by the O($2p_z$) orbital, with contributions from the $2p_z$ and $2p_x$ orbitals of C(4) and C(5) as well as the $2p_y$ orbitals of C(3) and C(2), which are enhanced by the 1s orbitals of H(8), H(6), H(9), and H(7). Because of the signs, the electron overlap forms two chains consisting of H(7)−C(4)−C(2) and H(9)−C(5)−C(3).

Although the overlap formed by the chains in the HOMO of the C_s conformer does not dominate the orbital wave function, the symmetry of the HOMO is affected significantly. When the pseudorotation angle starts to change, $\phi \neq 0°$, the electron overlap of the chains consisting of H(7)−C(4)−C(2) and H(9)−C(5)−C(3) starts to get distorted and then to break (electron overlap breaks not the bond), causing significant orbital symmetry changes. Specifically, the lefthand side chain of H(7)−C(4)−C(2) breaks first at $\phi = 45°$ (C_1), followed by a break of the right-hand side chain of H(9)−C(5)−C(3) at $\phi = 90°$ (C_2). The symmetry of the HOMO changes from a symmetric orbital (12a′ in C_s) to an asymmetric orbital (20a in C_1) and finally an antisymmetric orbital (9b in C_2). At $\phi = 90°$ (C_2), the O(2p) orbital and the CH_2 fragments on both sides of the oxygen atom, which formed a pair of p-like orbitals, result in the bell-shaped orbital MDs in part (a) of Figure 5 (the line at 90°).

IV.4. Other Valence Orbitals of THF. The other spectral peaks presented in the binding energy spectra in Figure 3 (bottom panel) and Table 1 can be divided into the outer valence region of IP < 18 eV and the inner valence region of IP ≥ 18 eV. At the experimental resolution of $\Delta E = 0.68$ eV, the spectral peaks are severely congested, except for the peak labeled 5 at 19.7 eV. As a result, fully resolved individual orbital MDs of THF are hardly obtained from the EMS experiment. Instead, clusters of the orbitals are obtained as follows. Orbitals 19−16 (Table 1) are assigned to peak 2 at 12.1 eV (Figure 3), orbitals 15−13 to peak 3, orbitals 12−11 to peak 4 and orbitals 10−9 to peak 5. Peaks 6, 7, and 8 (the satellites) at 23.4, 24.6, and 31.8 eV respectively are tentatively assigned to orbitals 8, 7, and 6 of THF, which are supported by the DFT-SAOP/et-pVQZ calculations.[18]

The observed clustered and theoretically synthesized orbital MDs for the outer valence space of THF are given in Figure 6. The theoretical MDs are calculated at the level of B3LYP/aug-cc-pVTZ and the procedures described by eqs 4 and 5 are used to take account of possible pseudorotation conformations in the simulations. Part (a) of Figure 6 reports the MDs of the clustered orbitals 19−16 related to peak 2 in the binding-energy spectrum. This profile exhibits two humps at approximately 0.30 au and 1.20 au respectively, and the synthesized theoretical ones reproduce the experimental features in general. According to the individually simulated orbital MDs using the DFT-SAOP/et-pVQZ model,[18] this cluster of orbitals is dominated by similar

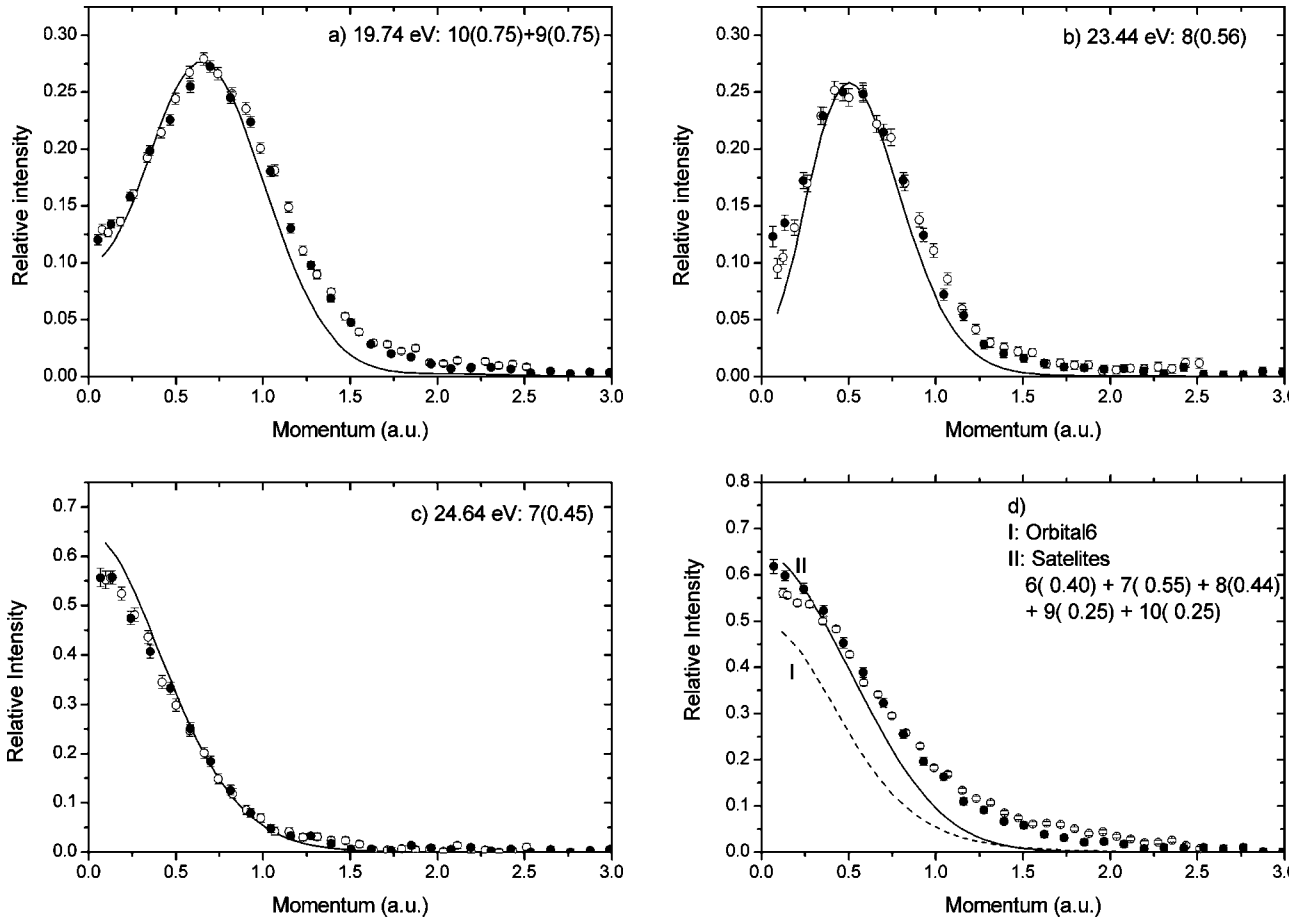

Figure 7. Comparison of the synthesized MDs of the inner valence orbitals of tetrahydrofuran (IP > 18 eV) with the observed spectra at an impact energy of 1200 eV (open circles) and 2400 eV (solid circles) plus binding energies, respectively. The measured pole strengths for these orbitals are given in the parentheses of Table 1.

shaped orbitals 17 and 18 plus a bell-shaped orbital 19 with its maximum intensity at approximately 1.20 au to enhance the second hump.

The next clustered orbitals consist of orbitals 15−13, associated with peak 3 at 14.5 eV. All of these orbitals are bell-shaped *p*-type orbitals,[18] as displayed in part (b) of Figure 6. Part (c) of Figure 6, assigned to orbitals 12 and 11 at 16.7 eV in binding energy, indicates a strong s-like character. The synthesized overall outer valence orbital MDs, as shown in part (d) of Figure 6, though the summation causes the loss of the most important structural information, indeed implying the dominance of the s-like bonding.

The inner valence region in the energy range of 18−37 eV of THF is related to orbitals 10−6 and their satellite lines. The pole strengths of the states (see Table 1) imply that a break down of the orbital picture [43,45] in this energy region. However, the DFT-SAOP/et-pVQZ calculations suggest the dominance of orbitals 10−6 over statistical averages. As a result, the assignments for the inner valence shell orbitals are given as peak 5 at 19.7 eV to the orbitals 10 and 9, peaks 6 and 7 at the energies of 23.4 and 24.6 eV, respectively, to orbital 8 and 7, accordingly, and finally, the satellite at 31.8 eV is approximated to orbital 6. Figure 7 reports the observed orbital MDs of inner valence shell orbitals and the simulated MDs.

The orbital pair at 19.7 and 23.4 eV is dominated by p-like orbitals, with bell-shaped MDs, whereas the last couple of inner valence orbitals at the energies of 24.6 and 31.8 eV, are s-dominant orbitals as they are dominated by 2s atomic orbitals.[18] The experimental orbital MDs obtained in the present work support the previous theoretical findings.[18] In Figure 7, a spectroscopic factor of the inner valence orbitals given in Table 1 has been employed to fit the theoretical simulations to the observed MDs.

The second last peak at the binding energy spectrum of THF in Figure 3 is not well resolved in the experiment but the deconvolution procedure has well disentangled their overlap. The orbital pair, orbitals 8 and 7, though close in energy, are associated with very different bonding types, in agreement with earlier theoretical results.[18] Parts (b) and (c) of Figure 7 reveal that orbital 8 is close to a p-type, in which the MDs displays a bell shape with a small residue at the momentum origin $I(p = 0) \rightarrow$small, whereas orbital 7 is an s-type, which exhibits a maximum at the momentum origin $I(p = 0) \rightarrow I_{max.}$

Two very broad Gaussian functions that appeared in the binding energy spectrum in Figure 3 at the energies of approximately 25 and 32 eV are likely satellites and therefore are used to approximate the accumulated intensities of the satellite lines. The simulated MDs (solid line) are given in part (d) of Figure 7 and the orbital MDs of the innermost valence orbital of THF. This orbital is irrelevant to pseudorotation, as this orbital is dominated by the 2s orbitals of carbon and oxygen atoms.[18] It is rather formidable to reproduce all of the satellite line with high level calculations, such as Green function theory (GF) or configuration interaction (CI), when the pseudorotation is considered. The theoretical simulation in part (d) of Figure 7 assumes that all satellite lines related to the inner valence space orbitals 10−7 are located at this energy region, and the satellite line has the same shape with its main line.[43,59] It is noted that

the theoretical maximum intensity ratio of the inner valance orbitals calculated using the DFT-SAOP/et-pVQZ model (Figure 5 of ref 18) is approximately I(orbital 10):I(orbital 9):I(orbital 8):I(orbital 7):I(orbital 6) = 3:3:5:15:10 respectively, that is, the s-like orbitals 7 and 6 dominate the MDs in this region, in agreement with the observed MDs given in part d of Figure 7.

V. Conclusions

The pseudorotation mechanism of THF has been investigated in the valence electron space using high-resolution EMS the first time. The orbital MDs of the valence orbitals of tetrahydrofuran are measured using the impact energies of 1200 and 2400 eV plus binding energies with an energy resolution of 0.68 eV. The present EMS experiment fully resolves the orbital MDs of the HOMO of THF, which is in good agreement with our earlier findings of the C_s conformer domination under the experimental conditions.[17]

The experimental findings are appropriately supported by the results from the B3LYP/aug-cc-pVTZ and OVGF/6−311++G** calculations, which agree well with a previous theoretical analysis for the conformations of THF.[18] The present study further incorporates thermodynamic population analysis, producing consistent results with the experimental measurements building up confidences in the theoretical models to further explore the pseudorotation mechanism from a nontradition point of view, that is, the momentum space. The orbital MDs of the HOMOs are then simulated as a function of the pseudorotation angle, ϕ, giving a v-shaped orbital MD cross section at $p = 0$ au (in fact, at any momentum p values with $p < 0.70$ au). Combined with the electron density distributions of the HOMOs in coordinate space, it reveals that the HOMO orbital MD variations in small momentum region are due to the distortion and break of electron overlap during pseudorotation. First, the H(7)−C(4)−C(2) chain breaks at $\phi = 45°$ of a C_1 conformation, and then the chain H(9)−C(5)−C(3) breaks at $\phi = 90°$ to produce a C_2 conformation, leading to the orbital symmetry changeover.

The synthesized clustered outer valence orbital MDs (due to energy resolution) exhibit good agreement with experiment, and so do the more discrete inner valence orbitals. The innermost valence orbital pair of orbitals 7 and 6, which are formed dominantly by the O2s and C2s orbitals,[18] are invariant with respect to the pseudorotation angle ϕ, which is in contrary to the HOMO, the outermost valence orbital of THF. It indicates that the pseudorotation mechanism of THF is orbital-dependent. To achieve a comprehensive understanding of pseudorotation and therefore the sugar puckering mechanism, orbital-based information must be investigated. The present study explores an innovative approach to study conformer-rich biological systems where the potential energy barriers are very low.

Acknowledgment. This work is supported by the National Natural Science Foundation of China under contract No. 10575062 and 10704046, and Specialized Research Fund for the Doctoral Program of Higher Education under 20050003084. F.W. acknowledges the Australian Research Council (ARC) for an International Linkage Award. This work was supported by an award under the Merit Allocation Scheme on the APAC National Facility at the ANU.

References and Notes

(1) Bouchiha, D.; Gorfinkiel, J. D.; Caron, L. G.; Sanche, L. J. *Phys. B: At. Mol. Opt. Phys.* **2006**, *39*, 975.
(2) Cadioli, B.; Gallinella, E.; Coulombeau, C.; Jobic, H.; Berthier, G. *J. Phy. Chem.* **1993**, *97*, 7844.
(3) Mozejko, P.; Sanche, L. *Radiat. Phys. Chem.* **2005**, *73*, 77.
(4) Jawetz, E. *Antiviral Chemotherapy and Prophylaxis. Basic and Clinical Pharmacology*, Katzung, B. G., Ed.; Appleton&Lange: Englewood Cliffs, NJ, 1992; p 674.
(5) Lafferty, W. J.; W. Robinnson, D.; St. Louis, R. V.; W. Russel, J.; Strauss, H. L. *J. Chem. Phys.* **1965**, *42*, 2915.
(6) Diez, E.; Esteban, A. L.; Bermejo, F. J.; Rico, M. J. *Phys. Chem.* **1980**, *84*, 3191.
(7) Seong, J. H.; Young, K. K. *THEOCHEM.* **1996**, *369*, 157.
(8) Meyer, R.; Lopez, J. C.; Alonso, J. L.; Melandri, S.; Favero, P. G.; Garminati, W. J. *Chem. Phys.* **1999**, *111*, 7871.
(9) Rayón, V. M.; Sordo, J. A. J. *Chem. Phys.* **2005**, *122*, 204303.
(10) Zecca, A.; Perazzolli, C.; Brunger, M. J. J. *Phys. B* **2005**, *38*, 2079.
(11) Tranter, G. E.; Macdermott, A. J. *Chem. Phys. Lett.* **1986**, *130*, 120.
(12) Melnik, D. G.; Gopalakrishnan, S.; Miller, T. A.; De Lucia, F. C. J. *Chem. Phys.* **2003**, *118*, 3589.
(13) Wu, A.; Cremer, D. *Int. J. Mol. Sci.* **2003**, *4*, 158.
(14) Engerholm, G. G.; Luntz, A. C.; Gwinn, W. D.; Harris, D. O. *J. Chem. Phys.* **1969**, *50*, 2446.
(15) Mamleev, A. H.; Gunderova, L. N.; Galeev, R. V. J. *Struct. Chem.* **2001**, *42*, 365.
(16) Luger, P.; Buschmanm, J. *Angew. Chem., Int. Ed.* **1983**, *22*, 410.
(17) Yang, T. C.; Su, G. L.; Ning, C. G.; Deng, J. K.; Wang, F.; Zhang, S. F.; Ren, X. G.; Huang, Y. R. *J. Phys. Chem. A* **2007**, *111*, 4927.
(18) Duffy, P.; Sordo, J. A.; Wang, F. J. *Chem. Phys.* **2008**, *128*, 125102.
(19) Wang, F. J. *Phys. Chem. A* **2003**, *107*, 10199.
(20) Jones, D. B.; Wang, F.; Brunger, M. J.; Winkler, D. A. *Biophys. Chem.* **2006**, *121*, 105.
(21) Jones, D. B.; Bolorizadeh, M. A.; Brunger, M. J.; Saha, S.; Wang, F.; Gleiter, R.; Bueber, J; Winkler, D. A. J. *Phys B: At., Mol. and Opt. Phys.* **2006**, *39*, 2411.
(22) Shan, X.; Chen, X. J.; Zhou, L. X.; Li, Z. J.; Liu, T.; Xue, X. X.; Xu, K. Z. J. *Chem. Phys.* **2006**, *125*, 154307.
(23) Takahashi, M.; Watanabe, N.; Khajuria, Y.; Udagaw, Y.; Eland, J. H. D. *Phys. Rev. Lett.* **2005**, *94*, 213202.
(24) Ning, C. G.; Ren, X. G.; Deng, J. K.; Su, G. L.; Zhang, S. F.; Huang, F.; Li, G. Q. *Chin. Phys.* **2005**, *14*, 2467.
(25) Ning, C. G.; Ren, X. G.; Deng, J. K.; Zhang, S. F.; Su, G. L.; Huang, F.; Li, G. Q. *Chem. Phys. Lett.* **2005**, *407*, 423.
(26) Ning, C. G.; Ren, X. G.; Deng, J. K.; Zhang, S. F.; Su, G. L.; Zhou, H.; Li, B.; Huang, F.; Li, G. Q. *Chem. Phys. Lett.* **2005**, *402*, 175.
(27) Lower, J.; Weigold, E.; Berakdar, J.; Mazevet, S. *Phys. Rev. Lett.* **2001**, *86*, 624.
(28) Neville, J. J.; Zheng, Y.; Brion, C. E. *J. Am. Chem. Soc.* **1996**, *118*, 10533.
(29) Deleuze, M. S.; Pang, W. N.; Salam, A.; Shang, R. C. *J. Am. Chem. Soc.* **2001**, *123*, 4049.
(30) Huang, Y. R.; Knippenberg, S.; Hajgato, B.; Francois, J. P.; Deng, J. K.; Deleuze, M. S. *J. Phys. Chem. A* **2007**, *111*, 5879.
(31) Saha, S.; Wang, F.; Falzon, C. T.; Brunger, M. J. *J. Chem. Phys.* **2005**, *123*, 124315.
(32) Wang, F. Electron Momentum Spectroscopy and Its Applications to Molecules of Biological Interest. In *Computational Methods in Sciences and Engineering, Theory and Computation: Old Problems and New Challenges*; Maroulis, G., Simos, T., Eds.; 2007, Vol. 1, pp 54−81.
(33) Wang, F.; Downton, M.; Kidwani, N. J. *Theor. Comp. Chem.* **2005**, *4*, 247.
(34) Brion, C. E. *Int. J. Quantum Chem.* **1986**, *29*, 1397.
(35) McCarthy, I. E.; Weigold, E. *Rep. Prog. Phys.* **1991**, *91*, 789.
(36) Weigold, E.; McCarthy, I. E. *Electron Momentum Spectroscopy*; Kulwer/Plenum: New York, 1999.
(37) Ning, C. G.; Ren, X. G.; Deng, J. K.; Su, G. L.; Zhang, S. F.; Li, G. Q. *Phys. Rev. A* **2006**, *73*, 022704.
(38) Ren, X. G.; Ning, C. G.; Deng, J. K.; Zhang, S. F.; Su, G. L.; Huang, F.; Li, G. Q. *Phys. Rev. Lett.* **2005**, *94*, 163201.
(39) Brion, C E; Zheng, Y; Rolke, J; Neville, J J; McCarthy, I E; Wang, J. *J. Phys. B* **1998**, *31*, L223.
(40) Takahashi, M; Saito, T; Hiraka, J; Udagawa, Y. *J. Phys. B* **2003**, *36*, 2539.
(41) Ning, C. G.; Ren, X. G.; Deng, J. K.; Zhang, S. F.; Su, G. L.; Huang, F.; Li, G. Q. *Chem. Phys. Lett.* **2005**, *407*, 423.
(42) Coplan, M. A.; Moore, J. H.; Doering, J. P. *Rev. Mod. Phys.* **1994**, *66*, 985.
(43) Cederbaum, L. S.; Domcke, W. *Adv. Chem. Phys.* **1977**, *36*, 205.
(44) Öhrn, Y.; Born, G. *Adv. Quantum Chem.* **1981**, *13*, 1.
(45) Ning, C. G.; Ren, X. G.; Deng, J. K.; Su, G. L.; Zhang, S. F.; Knippenberg, S.; Deleuze, M. S. *Chem. Phys. Lett.* **2006**, *421*, 52.
(46) Bawagan, A. O.; Brion, C. E.; Davison, E. R.; Feller, D. *Chem. Phys.* **1987**, *113*, 19.
(47) Duffy, P.; Chong, D. P.; Casida, M. E.; Salahub, D. R. *Phys. Rev. A* **1994**, *50*, 4704.

(48) Zheng, Y.; Brion, C. E.; Brunger, M. J.; Zhao, K.; Grisogono, A. M.; Braidwood, S.; Weigold, E.; Chakravorty, S. J.; Davidson, E. R.; Sgamellotti, A.; von Niessen, W. *Chem. Phys.* **1996**, *212*, 269.

(49) Duffy, P.; Casida, M. E.; Brion, C. E.; Chong, D. P. *Chem. Phys.* **1992**, *159*, 347.

(50) Hollebone, B. P.; Neville, J. J.; Zheng, Y.; Brion, C. E.; Wang, Y.; Davidson, E. R. *Chem. Phys.* **1995**, *196*, 13.

(51) Lee, C.; Yang, W.; Parr, R. G. *Phys. Rev. B* **1988**, *37*, 785.

(52) Frisch, M. J. et al., *Gaussian03, revision D02*; Gaussian Inc: Pittsburgh, PA, 2003.

(53) Ning, C. G.; Hajgató, B.; Huang, Y. R.; Zhang, S. F.; Liu, K.; Luo, Z. H.; Knippenberg, S.; Deng, J. K.; Deleuze, M. S. *Chem. Phys.* **2008**, *343*, 19.

(54) Ren, X. G.; Ning, C. G.; Deng, J. K.; Zhang, S. F.; Su, G. L.; Huang, F.; Li, G. Q. *Rev. Sci. Instrum.* **2005**, *76*, 063103.

(55) Ning, C. G.; Deng, J. K.; Su, G. L.; Zhou, H.; Ren, X. G. *Rev. Sci. Instrum.* **2004**, *75*, 3062.

(56) Ning, C. G.; Zhang, S. F.; Deng, J. K.; Liu, K.; Huang, Y. R.; Luo, Z. H. *Chin. Phys.* **2008**, *17*, 1674.

(57) Ning, C. G.; Ren, X. G.; Deng, J. K.; Zhang, S. F.; Su, G. L.; Huang, F.; Li, G. Q *J. Chem. Phys.* **2005**, *122*, 224302.

(58) Kimura, K.; Katsuwata, S.; Achiba, Y.; Yamazaki, T.; Iwata, S. *Handbook of HeI Photoelectron Spectra of Fundamental Organic Molecules*; Halsted Press: New York, 1981.

(59) Brunger, M. J.; McCarthy, I. E.; Weigold, E. *Phys. Rev. A* **1999**, *59*, 1245.

(60) Molden was written by G., Schaftenaar *CAOS/CAMM Center Nijmegen Toernooiveld, Nijmegen*; The Netherlands, 1991.

JP8038658